Uncoupling DNA damage from chromatin damage to detoxify doxorubicin

Xiaohang Qiao[a,b,1,2], Sabina Y. van der Zanden[c,1], Dennis P. A. Wander[d], Daniel M. Borràs[c], Ji-Ying Song[e], Xiaoyang Li[f], Suzanne van Duikeren[g], Noortje van Gils[h], Arjo Rutten[h], Tessa van Herwaarden[c], Olaf van Tellingen[i], Elisa Giacomelli[j], Milena Bellin[j], Valeria Orlova[j], Leon G. J. Tertoolen[j], Sophie Gerhardt[k], Jimmy J. Akkermans[c], Jeroen M. Bakker[c], Charlotte L. Zuur[b], Baoxu Pang[c], Anke M. Smits[c], Christine L. Mummery[j], Linda Smit[h], Ramon Arens[g], Junmin Li[f,2], Hermen S. Overkleeft[d], and Jacques Neefjes[c,2]

[a]Division of Tumor Biology and Immunology, The Netherlands Cancer Institute, 1066 CX Amsterdam, The Netherlands; [b]Department of Head and Neck Oncology and Surgery, The Netherlands Cancer Institute, 1066 CX Amsterdam, The Netherlands; [c]Department of Cell and Chemical Biology, ONCODE Institute, Leiden University Medical Center, 2333 ZC Leiden, The Netherlands; [d]Leiden Institute of Chemistry, Leiden University, 2300 RA Leiden, The Netherlands; [e]Division of Experimental Animal Pathology, The Netherlands Cancer Institute, 1066 CX Amsterdam, The Netherlands; [f]Department of Hematology, Shanghai Institute of Hematology, National Research Center for Translational Medicine, RuiJin Hospital affiliated to Shanghai Jiao Tong University School of Medicine, 200025 Shanghai, China; [g]Department of Immunohematology and Blood Transfusion, Leiden University Medical Center, 2333 ZA Leiden, The Netherlands; [h]Department of Hematology, Vrije Universiteit Medical Center, Cancer Center Amsterdam, 1081 HV Amsterdam, The Netherlands; [i]Division of Diagnostic Oncology, The Netherlands Cancer Institute, 1066 CX Amsterdam, The Netherlands; [j]Department of Anatomy and Embryology, Leiden University Medical Center, 2333 ZC Leiden, The Netherlands; and [k]Central Laboratory Animal Facility, Leiden University Medical Center, 2333 ZC Leiden, The Netherlands

The anthracycline doxorubicin (Doxo) and its analogs daunorubicin (Daun), epirubicin (Epi), and idarubicin (Ida) have been cornerstones of anticancer therapy for nearly five decades. However, their clinical application is limited by severe side effects, especially dose-dependent irreversible cardiotoxicity. Other detrimental side effects of anthracyclines include therapy-related malignancies and infertility. It is unclear whether these side effects are coupled to the chemotherapeutic efficacy. Doxo, Daun, Epi, and Ida execute two cellular activities: DNA damage, causing double-strand breaks (DSBs) following poisoning of topoisomerase II (Topo II), and chromatin damage, mediated through histone eviction at selected sites in the genome. Here we report that anthracycline-induced cardiotoxicity requires the combination of both cellular activities. Topo II poisons with either one of the activities fail to induce cardiotoxicity in mice and human cardiac microtissues, as observed for aclarubicin (Acla) and etoposide (Etop). Further, we show that Doxo can be detoxified by chemically separating these two activities. Anthracycline variants that induce chromatin damage without causing DSBs maintain similar anticancer potency in cell lines, mice, and human acute myeloid leukemia patients, implying that chromatin damage constitutes a major cytotoxic mechanism of anthracyclines. With these anthracyclines abstained from cardiotoxicity and therapy-related tumors, we thus uncoupled the side effects from anticancer efficacy. These results suggest that anthracycline variants acting primarily via chromatin damage may allow prolonged treatment of cancer patients and will improve the quality of life of cancer survivors.

doxorubicin | cardiotoxicity | therapy-related tumors | chromatin damage | DNA damage

The anthracycline doxorubicin (also known as Adriamycin, Doxo) and its analogs daunorubicin (Daun), epirubicin (Epi), and Idarubicin (Ida) are widely used in the treatment of various hematologic malignancies and solid tumors, as monotherapies or main ingredients in combination therapies with other drugs or antibodies (1, 2). As with many other chemotherapeutics, anthracyclines can cause severe side effects in patients, most notably, dose-dependent irreversible cardiotoxicity, which can be lethal. Upon reaching the maximal cumulative dose, alternative treatment strategies are needed if any are available (3–5). The risk of cardiotoxicity increases with age extremes (6) and also limits anthracycline treatment of recurring tumors, even if these drugs could still be effective (7–10). As a result, elderly cancer patients with a "weak heart" are often excluded from chemotherapy regimens containing anthracyclines

(11, 12). Moreover, combination with other drugs or radiotherapy in the heart region further increases the incidence of anthracycline-related cardiotoxicity (13).

Besides cardiotoxicity, Doxo causes other serious side effects. Particularly devastating are therapy-related tumors (14, 15). Roughly 1 to 3% of juvenile patients and 0.2 to 1% of breast cancer patients develop therapy-related tumors within 5 y after the initial anthracycline-containing treatment (16, 17). Therapy-related tumors are frequently associated with high-risk cytogenetics with a significantly lower rate of complete remissions

Significance

Anthracyclines like doxorubicin are anticancer drugs, used by over 1 million cancer patients annually. However, they cause severe side effects, most notably, cardiotoxicity and therapy-related malignancies. It is unclear whether these side effects are directly linked to their anticancer activity. Doxorubicin exerts two activities: DNA damage and chromatin damage. Here, we show that both activities conspire in the cardiotoxicity, while doxorubicin variants with only chromatin-damaging activity remain active anticancer drugs devoid of side effects. This challenges the concept that doxorubicin works primarily by inducing DNA double-strand breaks and reveals another major anticancer activity, chromatin damage. Translating these observations will yield anticancer drugs for patients that are currently excluded from doxorubicin treatment and improve the quality of life of cancer survivors.

(CRs) than de novo tumors (18–20). The third major side effect impacting quality of life is infertility (21). Therefore, sperm or ova of young cancer patients are frequently collected and preserved prior to anthracycline-based chemotherapy for later fertility treatment.

It is unclear whether the anticancer activities of anthracyclines are intimately coupled to their various side effects. The anthracyclines are topoisomerase II (Topo II) poisons, whereby they induce DNA double-strand breaks (DSBs) (22). While Doxo and related anthracyclines show high efficacy in the clinic, etoposide (Etop), a structurally unrelated Topo II poison which also generates DSBs (23), is significantly less potent in tumor control (24, 25) and less cardiotoxic (26). This suggests that DNA damage as a result of Topo II poisoning does not fully account for the clinical effects and cardiotoxicity. More recently, anthracyclines unlike Etop have been shown to evict histones from particular regions in the genome (24, 27, 28). Histone eviction by anthracyclines has multiple consequences, including epigenomic and transcriptional alterations and attenuated DSB repair, collectively referred to as *chromatin damage* (24, 29). These studies identified a variant anthracycline, aclarubicin (Acla), that evicts histones but fails to induce DSBs (24, 29). This drug is an effective anticancer drug, particularly for the treatment of acute myeloid leukemia (AML) (7, 30, 31).

Here, we reveal that the combination of DNA and chromatin damage assembled in Doxo and its variants is responsible for the different side effects. By understanding the effective chemical structure of each activity, we synthesized and identified analogs that failed to induce DSBs, but maintained histone eviction activity. These analogs abstained from causing therapy-related tumors and cardiotoxicity in mice and human cardiac microtissues, while retaining significant anticancer activity. This suggests that chromatin damage is apparently an important chemotherapeutic activity of anthracyclines, which—when separated from DSB formation—can ameliorate treatment-limiting side effects in mice. Consequently, anthracyclines can be detoxified by chemically removing the DNA-damaging effect while maintaining their chromatin-damaging activity. This provides different strategies for anthracycline development and a rationale for a more intense and broader application of anthracycline variants in the clinic.

Results

The Combination of DNA- and Chromatin-Damaging Activities Accelerates Tumor Formation and Causes Tissue Toxicities in Mice.
In addition to treatment-limiting cardiotoxicity, Doxo-containing chemotherapy induces treatment-related tumors in close to 1% of cancer survivors (16, 17). To explore the molecular basis of the different side effects of anthracyclines, we tested the in vivo carcinogenicity and cardiotoxicity of Doxo, in parallel with its analog Acla, capable only of chromatin damage, and Etop—a nonanthracycline drug proficient in DSB induction via Topo II but incapable of chromatin damage (24). $Trp53^{+/-}$ FVB mice [a spontaneous mouse tumor model (32–34)] were treated six times at 2-wk intervals with Doxo, Acla, Etop, or saline at a drug dosage and treatment schedule corresponding to standard patient therapy (24, 35). As in clinic practice, animals recovered from drug treatment within the 2-wk intervals, and no death was caused by acute toxicities. These mice were then followed for tumor development and long-term toxicities up to 72 wk (Fig. 1A). Doxo-treated mice presented accelerated death due to tumor formation, excluding 10 out of 32 Doxo-treated mice, who died from cardiotoxicity prior to development of detectable tumors. In contrast, Acla-treated mice showed attenuated spontaneous tumor formation, while Etop treatment moderately accelerated this process (Fig. 1 B and C). Since DNA mutations are a major driver of cancer (36), the difference in tumor formation for the three drugs could be a dose-dependent result of DNA errors introduced during inaccurate damage repair. Although Doxo and Etop both induce DSB, the damage is further exacerbated by the chromatin-damaging activity

of Doxo (24). Detailed histopathological analysis revealed that, among a variety of tumor types developed in $Trp53^{+/-}$ mice, high incidence of breast cancer was observed in 65% (11 out of 17) of Doxo-treated female mice, while the tumor spectra of Etop- and Acla-treated mice were comparable to that of saline-treated mice (*SI Appendix*, Table S1 and Fig. S1 *A and B*). This observation may explain the increased risk for breast cancer observed in juvenile cancer survivors with a history of anthracycline-based therapies (37, 38). Hence, the combination of DSB formation with chromatin damage induction, as for Doxo, enhances tumor formation, while removal of this, as for Acla, alleviates induction of therapy-related tumors.

Similar to human patients (3, 39), cumulative dose and male gender were also risk factors for Doxo-induced cardiotoxicity in mice (*SI Appendix*, Fig. S1 *C–G*). Histopathological analysis revealed substantial and exclusive heart damage in 78.1% of Doxo-treated mice, commonly presented as thrombus formation in the left atrium and auricle of the heart accompanied by inflammation and fibrosis (40, 41) (Fig. 1 *D–F* and *SI Appendix*, Fig. S1H). Sirius Red staining highlights these lesion areas showing increased levels of collagen (Fig. 1 *G and H*), while further staining for desmin, vimentin, and periostin showed impairment of myocytes (*SI Appendix*, Fig. S2 *A and B*) and increased fibrous stroma (*SI Appendix*, Fig. S2 *C–I*). Up-regulation of periostin was also observed in the myocardium of ventricles in Doxo-treated mice, particularly, in the left ventricles and septums (*SI Appendix*, Fig. S2 *F and I*). These alterations are known to be associated with anthracycline-induced chronic cardiotoxicity (42, 43). Postmortem histopathological analysis of all other major organs revealed severe dose-dependent effects on spermatogenesis in Doxo-treated male mice only (Fig. 1I and *SI Appendix*, Fig. S2 *J–P*), another known side effect of anthracyclines. These mouse experiments recapitulate three foremost long-term side effects of Doxo known in human patients and other animal models, suggesting that uncoupling DNA- from chromatin-damaging activity of anthracyclines could alleviate side effects, as this combination is absent in Etop and Acla.

Chromatin- and DNA-Damaging Activities Can Be Uncoupled in Anthracyclines.
The anthracyclines Doxo, Daun, Epi, and Ida all combine DNA-damaging and chromatin-damaging activities (24). A recently developed anthracycline analog, amrubicin (Amr), was reported with limited cardiotoxicity (44). We tested the DNA- and chromatin-damaging activities of Amr at physiologically relevant concentrations (24, 45). DNA damage was visualized by constant-field gel electrophoresis (CFGE) (46, 47), comet assay (48), and phosphorylation of H2AX at Ser139 (γH2AX) (49). Amr, Doxo, Daun, Epi, Ida, and Etop all induced DSBs, unlike Acla (Fig. 2 *A–E* and *SI Appendix*, Fig. S3 *A–C*). Subsequently, chromatin damage was detected after photo-activation of green fluorescent protein-labeled histone H2A (PAGFP-H2A) in living cells (24). Only Amr and Etop failed to evict histones (Fig. 2 *F and G*, *SI Appendix*, Fig. S3D, and Movie S1). The anthracycline Amr thus mimicked Etop, which only induces DSBs. Amr and Etop both have limited cardiotoxicity (26, 44, 50), again suggesting that DNA damage alone is insufficient to induce cardiotoxicity.

Relocation of the amine group from the sugar (as found in Doxo) to the tetracycline moiety in Amr disabled histone eviction (Fig. 2A), but still allowed induction of DSBs, suggesting that the amine on the sugar of Doxo is crucial for evicting histones. Furthermore, Acla whose amine group is present at the same position but in a dimethylated form exhibited only histone eviction activity without DSB induction (Fig. 2 *A–G*). To identify the structural basis of these two cellular activities of Doxo, we synthesized and tested *N,N*-dimethyldoxorubicin (diMe-Doxo) (*Materials and Methods* and *SI Appendix, Method S1*). *N,N*-dimethylation of the amine group in Doxo abolished
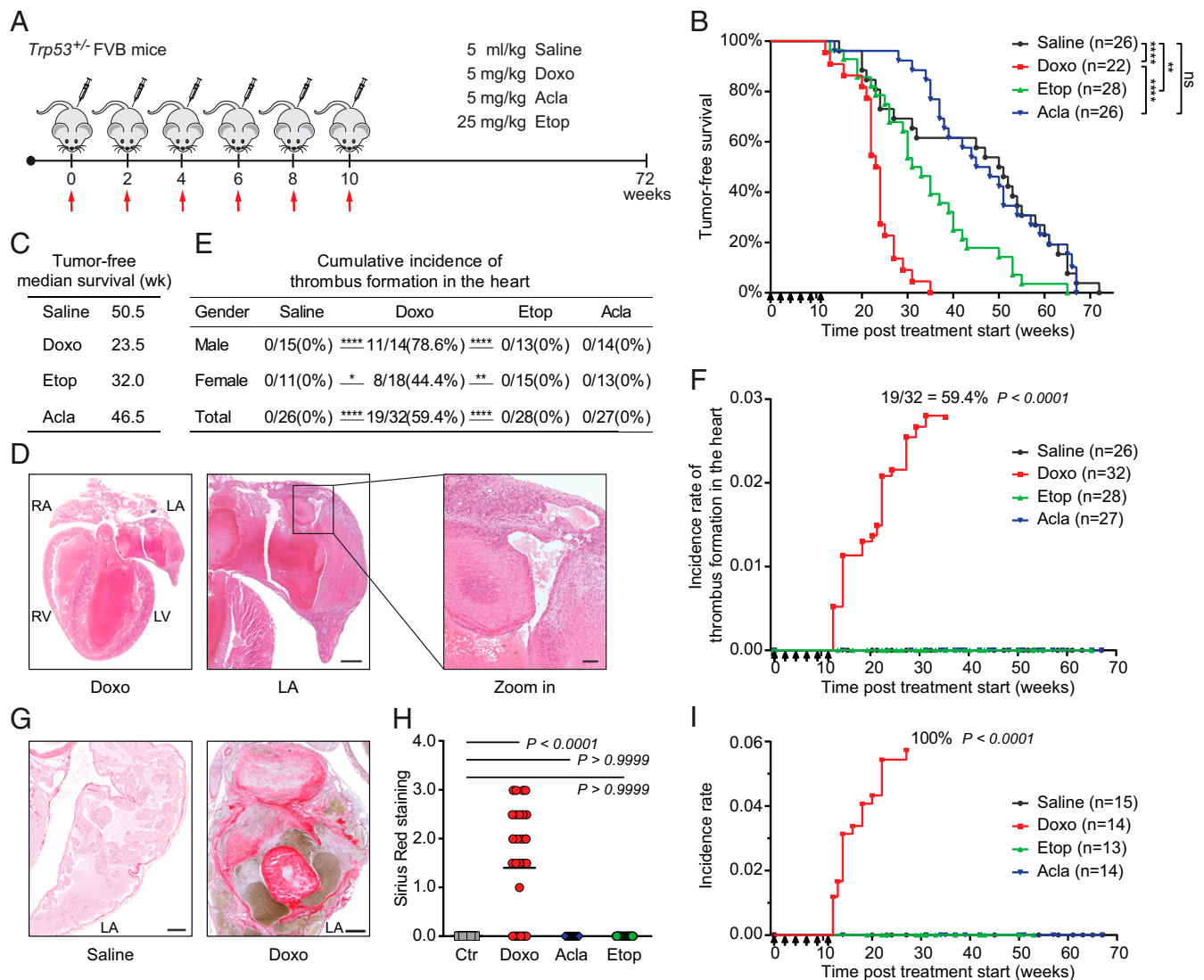
Fig. 1. Doxo and Etop, but not Acla, accelerate tumor formation and Doxo causes tissue toxicities in *Trp53*^{+/−} FVB mice. (*A*) *Trp53*^{+/−} FVB mice were i.v. injected with Doxo, Acla, Etop, or saline every 2 wk for six times. Drug injections are indicated by arrows. (*B*) Tumor-free survival is plotted in a Kaplan−Meier curve. Drug injections are indicated by arrows. Log-rank test, ns, not significant; ****$P < 0.0001$; **$P = 0.0093$. (*C*) Tumor-free median survival of mice. (*D*) Representative microscopic images of the heart from Doxo-treated mouse with thrombosis formation in the left atrium/auricle. Higher magnifications shows thrombi and inflammatory lesions including fibrosis in the left auricle. LA, left atrium; RA, right atrium; LV, left ventricle; RV, right ventricle. (Scale bars, 500 μm and 100 μm, respectively.) (*E*) Cumulative incidence of thrombosis was analyzed for gender effect. Fisher's exact test, two-sided. *$P < 0.05$; **$P < 0.01$; ****$P < 0.0001$. (*F*) The incidence rate of thrombus formation in the heart. Drug injections are indicated by arrows. Cumulative incidence is indicated next to the curve. Two-way ANOVA with repeated measures (RM). (*G*) Representative Sirius Red staining of the LA from saline- or Doxo-treated mouse. (Scale bars, 100 μm.) (*H*) Quantification of Sirius Red staining. Kruskal−Wallis test. (*I*) Incidence rate of depletion of spermatogenesis in male mice. Drug injections are indicated by arrows. Cumulative incidence is indicated next to the curve. Two-way ANOVA with RM.

DNA-damaging activity at various concentrations (Fig. 2 *A*−*E* and *SI Appendix*, Fig. S3 *A*−*C*), while still allowing histone eviction (Fig. 2 *F* and *G*, *SI Appendix*, Fig. S3 *E*−*I*, and Movie S2). Further, the evicted H2B accumulated in the cytosolic fraction upon treatment of Doxo, diMe-Doxo, and Acla but not for Amr and Etop (Fig. 2 *H* and *I* and *SI Appendix*, Fig. S4 *A* and *B*). The diMe-Doxo still relocated Topo IIα-GFP to chromatin (*SI Appendix*, Fig. S4*C*), indicating that Topo IIα was trapped by the drug before the generation of DSB. These data suggest that manipulating the position and modification of the amine group in Doxo allows separation of the DNA-damaging and chromatin-damaging activities.

We then tested the relative contributions of DNA damage and chromatin damage to the anticancer effects of Doxo by assaying the cytotoxicity of these variants in different cancer cell lines

(Fig. 2 *J* and *K* and *SI Appendix*, Fig. S5*A*). The diMe-Doxo showed comparable or even superior effects in most cell lines tested compared to Doxo (14 out of 20), while Amr was poorly cytotoxic (Fig. 2*J*). This increased potency of diMe-Doxo in these cell lines was unexpected, given that this compound lost its DNA-damaging activity. This enhanced potency could not be attributed to the rate of drug uptake as analyzed by flow cytometry following the autofluorescence of the anthracycline drugs (*SI Appendix*, Fig. S5*B*). Reactive oxygen species (ROS) induced by anthracyclines was observed to be dose dependent but only at late time point after drug removal (*SI Appendix*, Fig. S6 *A* and *B*), indicating that it could be a secondary effect of drug action. ROS can cause many vicious damages, which might be responsible for the cell death induced by anthracyclines. Although the different anthracyclines induced some increase in
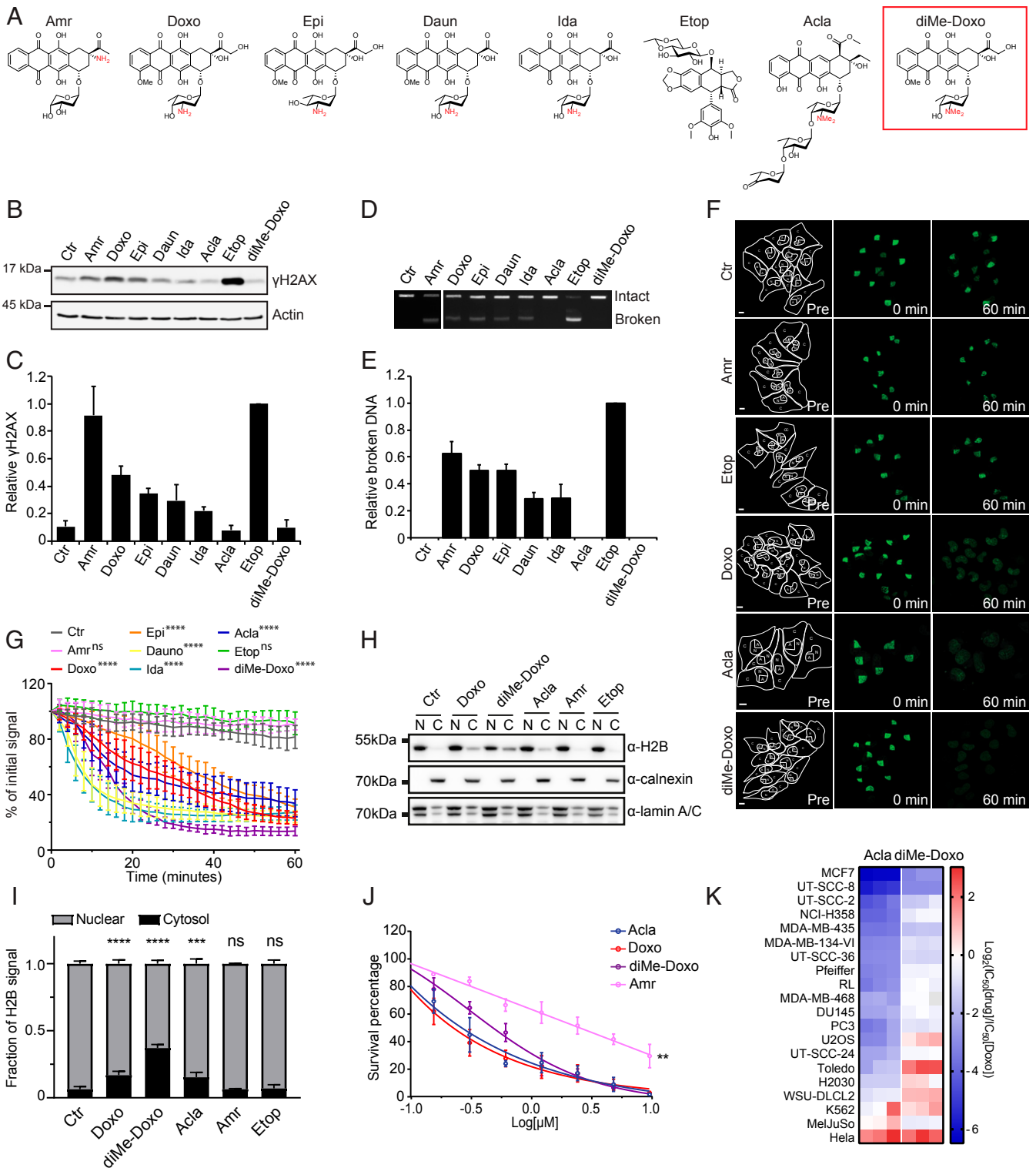
Fig. 2. Evaluation of the DNA- and chromatin-damaging activities of anthracyclines. (*A*) Structures of Topo II poisons used in this study, with the critical amine group in red. (*B*) K562 cells were treated for 2 h with 10 μM indicated drug. γH2AX levels were examined by Western blot. (*C*) Quantification of the γH2AX signal normalized to actin. (*D*) DSBs were analyzed by CFGE. (*E*) Quantification of relative broken DNA in *D*. (*F*) Part of the nucleus from MelJuSo-PAGFP-H2A cells was photoactivated. Photoactivated PAGFP-H2A was monitored by time-lapse confocal microscopy for 1 h in the absence or presence of indicated drug at 10 μM. Lines in Pre column define the regions of cytoplasm (C), nucleus (N), and activated area (A). (Scale bar, 10 μm.) (*G*) Quantification of the release of fluorescent PAGFP-H2A from the photoactivated region after drug administration. Two-way ANOVA, ****$P < 0.0001$. (*H*) Endogenously tagged scarlet-H2B U2OS cells were treated with 10 μM indicated drugs. Cells were fractionated, and the nuclear versus cytosolic fraction of H2B was examined by Western blot. Calnexin was used as cytosolic, and lamin A/C was used as nuclear marker. (*I*) The fraction of cytosolic versus nuclear H2B upon histone eviction by the drugs indicated is plotted. Two-way ANOVA, ***$P < 0.001$; ****$P < 0.0001$; ns, not significant. (*J*) Cell viability in K562 cells. Two-way ANOVA, Amr vs. Doxo, diMe-Doxo or Acla, **$P < 0.01$. (*K*) Relative IC$_{50}$ values of each drug compared to Doxo in different cell lines.

total ubiquitinated proteins, there was no significant difference observed for the different drugs (*SI Appendix*, Fig. S6 *C* and *D*). Besides ROS induction, chromatin damage-induced cell death is probably executed by classical caspase-dependent apoptosis, as shown by Poly ADP-ribose polymerase (PARP) cleavage following exposure to these drugs (*SI Appendix*, Fig. S6 *E* and *F*).

Anthracyclines That Only Evict Histones Are Effective in Cancer Treatment. To assess the importance of chromatin damage for the clinical activity of anthracyclines, we performed a retrospective analysis in de novo geriatric AML patients, who were treated with either Ida-based (that

induces both DSBs and chromatin damage) or Acla-based regimens (with chromatin damage only). Acla is reported to be equipotent to Daun for AML patients (30, 31); likewise, Acla-based regimen resulted in overall survival comparable to Ida-based regimen (Fig. 3*A* and *SI Appendix*, Fig. S7*A* and Tables S2 and S3), indicating that anthracycline drugs lacking DNA-damaging activity are effective in cancer treatment. The direct anticancer activity of diMe-Doxo compared to Doxo was evaluated ex vivo in primary human AML blasts (Fig. 3 *B* and *C* and *SI Appendix*, Fig. S7 *B–H*). Although some patient-to-patient variation existed, Doxo and diMe-Doxo were equally effective, while Acla appeared more cytotoxic in these
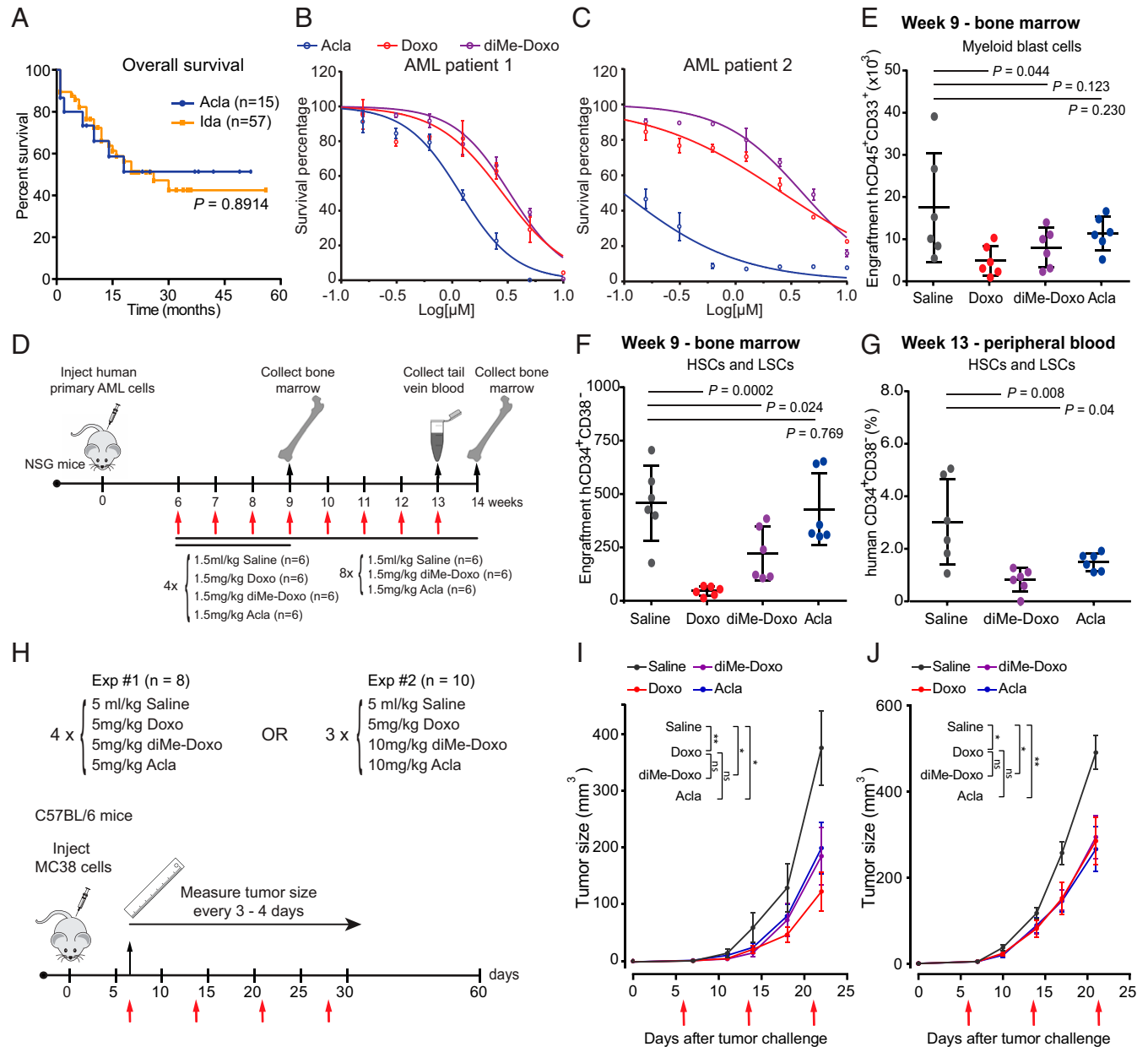
Fig. 3. Both diMe-Doxo and Acla are effective anticancer drugs. (*A*) Overall survival of de novo geriatric AML patients treated with a drug regimen including Acla or Ida. Log-rank (Mantel–Cox) test. (*B* and *C*) Dose-dependent cell viability of human AML samples, shown as mean ± SD of technical duplicates. (*D*) Schematic overview of AML PDX mouse experiment. (*E* and *F*) The engraftment of human AML cells in the BM of the first cohort at week 9: absolute counts of (*E*) myeloid blast cells (CD45⁺CD33⁺ blasts) and (*F*) HSCs and LSCs (CD34⁺CD38⁻ blasts). Each symbol represents one mouse. (*G*) The engraftment of human AML cells of the second cohort: the percentage of human HSCs and LSCs in PB at week 13. Student's' *t* test. (*H*) C57BL/6 mice were s.c. injected with MC38 cells. One week after tumor challenge, mice were treated with indicated drugs every week. Drug injections are indicated by arrows. (*I* and *J*) MC38 tumor growth following (*I*) experiment 1 procedure or (*J*) experiment 2 procedure. One-way ANOVA, saline vs. treatment, *$P < 0.05$; **$P < 0.01$.

Qiao et al.

dose–response experiments (Fig. 3 B and C and *SI Appendix*, Fig. S7 B–H). Chromatin-damaging activity apparently contributes significantly to the cytotoxicity of Doxo in treating AML.

The anticancer activity of diMe-Doxo in vivo was tested in an AML patient-derived xenograft (PDX) mouse model (51) in comparison to Doxo and Acla (Fig. 3D). Due to severe toxicity, mice treated with Doxo had to be killed after four courses of treatment at week 9, unlike mice treated with Acla or diMe-Doxo (*SI Appendix*, Fig. S8A), which then received another four courses of treatment without any signs of toxicity (Fig. 3D and *SI Appendix*, Fig. S8B). At week 9, four courses of Doxo treatment significantly depleted human AML blast cells, hematopoietic stem cells (HSCs), and leukemic stem cells (LSCs) (Fig. 3 E and F and *SI Appendix*, Fig. S8C), and showed modest but not significant impact on normal mouse leukocytes (*SI Appendix*, Fig. S8D). The diMe-Doxo and Acla did reduce the leukemic burden, albeit less efficiently than Doxo (Fig. 3 E and F). With extended treatment of diMe-Doxo and Acla, most proliferating fractions of human hematopoietic cells were significantly reduced in mice (Fig. 3G and *SI Appendix*, Fig. S8 E–H). The PDX experiment suggests that diMe-Doxo has the capacity to reduce the leukemic burden, the immature LSCs, and leukemic progenitors in vivo with less hematopoietic toxicity compared to Doxo. Subsequently, we tested a solid colon carcinoma tumor mouse model for the efficacy of the different anthracyclines that either do or do not induce DSBs (Fig. 3H). Both diMe-Doxo and Acla showed significant tumor control, although Doxo was slightly but not significantly better at reducing the tumor growth at equal dose (Fig. 3I). A higher dose of diMe-Doxo and Acla resulted in equal tumor control (Fig. 3J). Taken together, Acla and diMe-Doxo (with chromatin-damaging activity only) are effective anticancer drugs in vitro and in vivo, suggesting that chromatin damage could provide a major contribution to the mechanism of anthracycline cytotoxicity.

N,N-dimethylation of Doxo Prevents Cardiotoxicity. Since diMe-Doxo resembles the activity of Acla in terms of evicting histones while not causing DSBs (*SI Appendix*, Fig. S9A), we wondered whether this also translates into reduced side effects. To address this, wild-type FVB mice were intravenously (i.v.) injected with Acla, Doxo, or diMe-Doxo every 2 wk (Fig. 4A). Mouse body weight was monitored as a representative parameter of general toxicity prior to each injection (35). While Doxo-treated mice significantly lost body weight and died from cardiotoxicity after eight injections, mice treated with diMe-Doxo remained healthy, with no weight loss or discomfort, even after 15 doses (Fig. 4 B and C and *SI Appendix*, Fig. S9B). Histopathology demonstrated that Doxo treatment induced severe cardiotoxicity as observed in $Trp53^{+/-}$ FVB mice (Fig. 1 and *SI Appendix*, Figs. S1 and S2). None of the mice treated with either diMe-Doxo or Acla showed abnormalities in the heart (Fig. 4C and *SI Appendix*, Fig. S9 C–J). The effects on cardiac function of mice were further evaluated by echocardiography. Doxo treatment resulted in a serious expansion of the left atrium with reduced fractional shortening (FS), left ventricular ejection fraction (EF), and cardiac output unlike any of the other treatments (Fig. 4 D–G and Movie S3). More direct (acute) cardiac cell damage and function impairment were assessed using human induced pluripotent stem cell (hiPSC)-derived cardiac microtissues (52–55). Doxo unlike Acla or diMe-Doxo significantly affected contraction amplitude and contraction duration 24 h posttreatment (Fig. 4H, *SI Appendix*, Fig. S9 K–N, and Movie S4). This suggested that cardiotoxicity can be the result from combining DNA and chromatin damage. This was directly tested by the combination of Amr (DNA damage only) and Acla (chromatin damage only), which reduced the contraction amplitude to some extent and significantly impaired the velocity of the microtissues, which reconstituted the cardiotoxicity of Doxo

in hiPSC-derived cardiac microtissues (Fig. 4 I–K). These differences in toxicity of the heart cannot be caused by a different biodistribution of the drugs, which was comparable for Doxo and diMe-Doxo (*SI Appendix*, Fig. S9 K and O). Unlike Acla, diMe-Doxo affected the male reproductive organs. The diMe-Doxo depleted spermatogenesis in all male mice and caused some Leydig cell hyperplasia but to a lesser extent than its parental drug Doxo, even at higher cumulative dose (*SI Appendix*, Fig. S9 P and Q). Significant toxicity in ovaries in young mice at early time points was observed only for Doxo-treated mice, shown as increased apoptosis in secondary and tertiary follicles (*SI Appendix*, Fig. S9 R–T). These results indicated that diMe-Doxo and Acla (with chromatin-damaging activity only) are less toxic than anthracyclines that induce both DNA and chromatin damage (such as Doxo), while remaining effective anticancer drugs.

Discussion

About 1 million cancer patients annually receive treatment with Doxo or its analogs Daun, Epi, or Ida. Unfortunately, anthracyclines cause severe side effects, particularly cardiotoxicity (3, 4). This side effect excludes (often elderly) patients with compromised heart function from receiving effective cancer treatments (56). Understanding and ultimately eliminating the root causes of this and other side effects of anthracyclines would thus greatly expand the application of these drugs in cancer treatment.

It has been suggested that ROS formation may be responsible for cardiotoxicity induced by anthracyclines (57, 58). However, coadministration of radical quenchers during anthracycline treatment did not ameliorate cardiotoxicity in clinical studies (59, 60). Moreover, high redox potential of Acla relative to that of Doxo or Daun (61) does not match Acla's lack of cardiotoxic effects. Our data also show that Acla and diMe-Doxo produce more ROS compared to Doxo (*SI Appendix*, Fig. S6A), rather suggesting that ROS induction cannot explain the differences in cardiotoxicity of anthracyclines studied here.

Mechanistically, cardiotoxic anthracyclines, such as Doxo, Daun, Epi, and Ida, constitute multifunctional agents capable of DNA damage (by poisoning Topo II and DSB formation) combined with chromatin damage (via histone eviction). The anticancer effects have been attributed to DNA damage, but the variants unable to induce DNA damage show equal anticancer potency in AML treatment. While therapy-related tumors can be understood as the consequence of delayed and unfaithful DNA damage repair (24), the cause of cardiotoxicity by anthracyclines is still unsolved. Failure of removing cardiotoxicity by chemical modification in the past led to different delivery strategies such as liposome-encapsulated Doxo, but with modest improvement and limited use in clinical practice (62). Here we show that cardiotoxicity associated with Doxo is alleviated in mice treated with drugs that either induce DSBs (Etop) or evict histones (Acla, diMe-Doxo). This effect is further confirmed in hiPSC-derived cardiac microtissues and by echocardiography, collectively implying that the combination of DNA and chromatin damage induces cardiotoxicity. Although Doxo is an exceptional drug that shows very similar pharmacokinetics in human and mouse (63), there remains some distance between our mouse models and humans. However, the long-term toxicities of Doxo, cardiotoxicity, infertility, and therapy-related tumorigenesis observed in our mouse models do correlate very well with clinical observations. With this promising result from mice, effort will be made to test this concept in other animal models and clinical trial.

Many chemical variations of anthracyclines have been synthesized before, including diMe-Doxo (64, 65). However, these drugs were only tested for their ability to induce DNA damage, which was considered the main mechanism of therapeutic efficacy for anthracyclines (66). Since chromatin damage was unknown at that time (24), many of the variants lacking DNA-damaging activity were not further developed. We propose
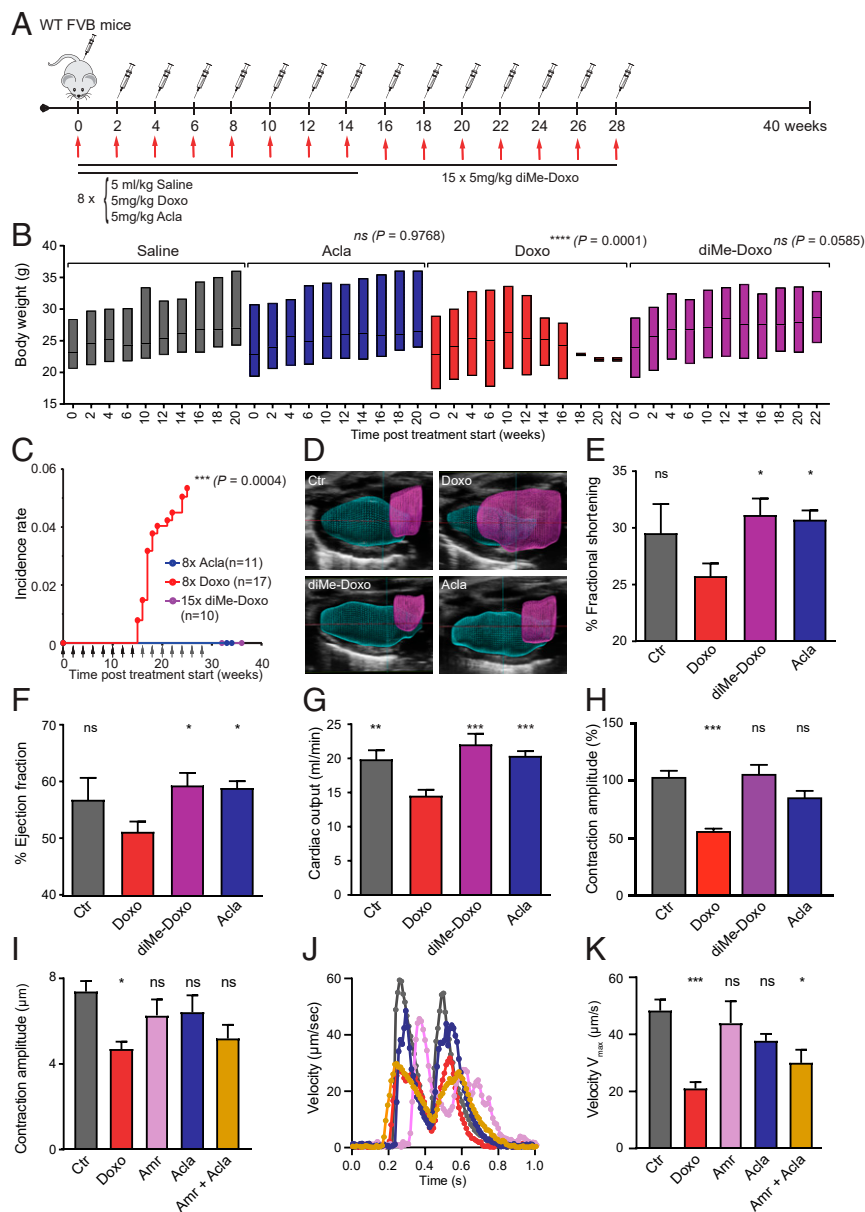
Fig. 4. *N,N*-dimethylation of Doxo prevents cardiotoxicity in mice and hiPSC-derived cardiac microtissues. (*A–C*) Wild-type (WT) FVB mice were i.v. injected with indicated drug every 2 wk: Doxo or Acla for 8 times and diMe-Doxo for 15 times. (*B*) The body weight of mice, shown as floating bars with maximum–median–minimum values. Two-way ANOVA with RM. (*C*) The incidence rate of cardiotoxicity. Arrows indicate drugs injections. Two-way ANOVA. (*D–G*) Cardiac function assessed by echocardiography 12 wk posttreatment start. FVB mice were treated for eight times with saline (5 mL/kg, *n* = 5), Doxo (5 mg/kg, *n* = 8), diMe-Doxo (5 mg/kg, *n* = 6), or Acla (5 mg/kg, *n* = 9). (*D*) A 3D reconstruction of the diastole heart by echocardiography. In the sagittal section, the left ventricle (cyan) and left atrium (magenta) are highlighted. (*E–G*) Quantification of echocardiography, (*E*) FS, (*F*) left ventricular EF, and (*G*) cardiac output. For *E–G*, ordinary one-way ANOVA, Doxo vs. saline, diMe-Doxo, or Acla, *P < 0.05; **P < 0.01; ***P < 0.001; ns, not significant. (*H*) Drug toxicity on cardiac microtissues 24 h posttreatment. Contraction amplitude of microtissues treated with 20 μM different drugs. Krushal–Wallis test, ***P < 0.0002. (*I–K*) Drug toxicity on cardiac microtissues treated with single drugs or a combination of Amr and Acla. (*I*) Contraction amplitude of microtissues treated with the indicated single (20 μM) or combination drugs (10 μM + 10 μM). (*J*) Maximum velocity in micrometers per second is indicated for a represented microtissue for the different treatments. (*K*) Quantification of the maximum velocity. For *I* and *K*, ordinary one-way ANOVA, Ctr vs. treatments; *P < 0.05; ***P < 0.001; ns, not significant.

that, by further understanding the cellular activities of anthracyclines, detoxification of Doxo is possible, which only requires a minimal chemical modification to remove the DNA-damaging activity. Such drugs would allow more intense treatment of primary tumors and continuous anthracycline treatment of relapsed tumors. Additionally, patients with higher cardiotoxicity risk, who are now excluded from anthracycline-based cancer treatments, may benefit from the detoxified anthracyclines. Evaluating old

anticancer drugs with modern technologies may lead to better understanding of drug activities (such as chromatin damage) that could then provide strategies for improvement of cancer therapies as exemplified—in this case—by diMe-Doxo. Chemical dissection of the cellular activities of Doxo uncovered a mechanism of action for anthracyclines—chromatin damage—and effective anticancer drugs devoid of the most critical side effects of anthracyclines.

Qiao et al.

Materials and Methods

Reagents. Doxo and Etop were obtained from Pharmachemie. Daun was obtained from Sanofi-Aventis. Epi was obtained from Accord Healthcare Limited. Acla for in vivo mouse experiment was purchased from Shenzhen Main Luck Pharmaceuticals Inc. All of the drugs were dissolved according to the manufacturer's formulation. Amr (sc-207289), Acla (sc-200160, for in vitro experiments), and Ida (sc-204774) were purchased from Santa Cruz Biotechnology, dissolved in dimethyl sulfoxide at 5 mg/mL concentration, aliquoted and stored at −20 °C for further use.

Synthesis of N,N-Dimethyldoxorubicin. All chemicals were used as received unless stated otherwise. The ^1H and ^{13}C NMR spectra were recorded on a 400/100 or 500/125 NMR spectrometer. Chemical shifts (δ) are given in parts per million relative to tetramethylsilane (TMS) as internal standard. Coupling constants are given in hertz. All given ^{13}C spectra are proton decoupled. Spin multiplicities are given as s (singlet), d (doublet), dd (doublet of doublets), ddd (doublet of doublet of doublets), dt (doublet of triplets), t (triplet), td (triplet of doublets), dt (doublet of triplets), q (quartet), dq (doublet of quartets), qd (quartet of doublets), h (heptet) and m (multiplet). All individual signals were assigned using two-dimensional (2D) NMR spectroscopy, HH-COSY (proton-proton correlated spectroscopy), and heteronuclear single quantum correlation. Flash chromatography was performed on Screening Device B.V. silica gel 60 (0.04 mm to 0.063 mm). TLC analysis (on Merck silica gel F254 plates) was followed by detection by ultraviolet absorption (254 nm) where applicable and by spraying with a solution of $(NH_4)_6Mo_7O_{24}·H_2O$ (25 g/L) and $(NH_4)_4Ce(SO_4)_4·2H_2O$ (10 g/L) in 10% sulfuric acid in water followed by charring at 275 °C. Liquid chromatography–mass spectrometry (LC-MS) standard eluents used were A: 100% H_2O, B: 100% acetonitrile, and C:1% TFA in H_2O. A C18 column (4.6 mm D × 50 mm L, 3-μ particle size) was used. All analyses were 13 min, at a flow-rate of 1 mL/min. High-resolution mass spectra were recorded on an LTQ-Orbitrap equipped with an electrospray ion source in positive mode (source voltage 3.5 kV, sheath gas flow 10, capillary temperature 275 °C) with resolution R = 60.000 atm/z = 400 (mass range = 150 to 4,000) and dioctylphthalate (m/z = 391.28428) as "lock mass." Size-exclusion chromatography was performed on Sephadex LH20 (eluent MeOH/DCM, 1:1). Detailed synthesis schemes can be found in *SI Appendix, Method S1*.

Cell Culture. K562 (B. Pang, Stanford University, Stanford, CA), THP-1 (ATCC, Manassas, VA), DU145 (C. Robson, Newcastle University, Newcastle, United Kingdom), NCI-H358, MBA-MD-468 (R. Bernards, Netherlands Cancer Institute [NKI], Amsterdam, The Netherlands), and Pfeiffer cells (ATCC, Manassas, VA) were maintained in RPMI-1640 medium supplemented with 8% fetal calf serum (FCS). MCF-7 (W. Zwart, NKI, Amsterdam, The Netherlands), U2OS cells (M. Innocenti, NKI, Amsterdam, The Netherlands), and MC38 cells (M. Colonna, Washington University School of Medicine, St. Louis, MO) were cultured in Dulbecco's modified Eagle's medium (DMEM) supplemented with 8% FCS. MelJuSo cells were cultured in Iscove's Modified Dulbecco's medium (IMDM) supplemented with 8% FCS. UT-SCC-8 cells (R. Grenman, University of Turku, Turku, Finland) were cultured in DMEM supplemented with 8% FCS and 1% nonessential amino acid. MelJuSo cells stably expressing PAGFP-H2A, PAGFP-H3, or PAGFP-H4 were maintained in IMDM supplemented with 8% FCS and G-418, as described (24). MelJuSo cells were transiently transfected with a construct encoding Topo IIα-GFP (24). Endogenous tagged scarlet-H2B cells were generated using a homology repair scarlet constructs, which was designed 250 base pairs upstream and downstream of the genomic H2BC11 region. The guide RNA (gRNA) target sequence was designed by the CRISPOR tool and cloned into the pX330 Cas9 vector. Primers used for the homologous recombination (HR) construct: H2B homology arm left fwd: CCCACATATGCAAGGTTCTGAAGCAGGTCCAC; H2B homology are as follows: arm left rev, CCCAGCTAGCCTTAGCGCTGGTGTACT TGG; H2B homology arm right fwd, CCCAGGTACCACAGTGAGTTGGTTGCA AAC; H2B homology arm right rev, CCCAGGATCCAACTTATAATAGAAAAT TTCCCATCTCC. Primers used for the pX330 Cas9 vector are as follows: H2B gRNA fwd, CACCGACTCACTGTTTACTTAGCGC; H2B gRNA rev, AAACGCGCT AAGTAAACAGTGAGTC. All cell lines were maintained in a humidified atmosphere of 5% CO_2 at 37 °C and regularly tested for the absence of mycoplasma.

Primary Human AML Cells Isolation and Culture. All studies were conducted in accordance with the Declaration of Helsinki, and the full study protocol was approved by the Ethics Committee of the Vrije Universiteit Medical Center (VUmc). At diagnosis, bone marrow (BM) or peripheral blood (PB) from AML patients hospitalized at the VUmc in Amsterdam, The Netherlands was collected with informed consent and according to protocols approved by the Ethics Committee of the VUmc. Mononuclear cells were isolated using Ficoll-Paque Plus (Amersham Biosciences). Primary AML cells were kept in IMDM supplemented with 15% BIT9500 (Stemcell Technologies), Pen-Strep, 50 ng/mL human FLT3 ligand, 20 ng/mL human IL3, and 100 ng/mL human stem cell factor (PeproTech).

Mouse Experiments for Assessing Drug Toxicities. Mice were housed in individually ventilated cages (IVC) under specific pathogen-free (SPF) conditions in the animal facility of the NKI (Amsterdam, The Netherlands). All mouse experiments were performed according to institutional and national guidelines and were approved by the Animal Ethics Committee of the NKI (Amsterdam, The Netherlands). $Trp53^{+/-}$ or wild-type FVB mice were bred by the NKI mouse facility. $Trp53^{+/-}$ FVB mouse strain and genotyping protocol were as described (32). Mice (10 wk to 11 wk old) were i.v. injected with 5 mg/kg of Doxo, 5 mg/kg of Acla, 5 mg/kg of diMe-doxo, 25 mg/kg of Etop, or 5 mL/kg of saline every 2 wk for the indicated times. Then tumor formation and animal welfare (weight loss, lethargy, hunched posture, poor grooming [rough hair coat]) were monitored every other day. When the tumor diameter exceeded 1 cm or the body weight loss was more than 20%, the animal was killed by CO_2. Subsequently, all organs and tumors were collected, fixed in EAF fixative (ethanol/acetic acid/formaldehyde/saline at 40:5:10:45 vol/vol), and embedded in paraffin. Sections were cut at 2 μm from the paraffin blocks and stained with hematoxylin and eosin, Sirius Red, or indicated antibodies according to standard procedures. Primary antibodies were Desmin (1:200, M 0760, DakoCytomation), Vimentin (1:100, #5741, Cell Signaling), and Periostin (1:100, ab215199, Abcam). The pathology slides were reviewed by an expert mouse pathologist who was blind to the treatment. Incidence rate (IR = [number of mice with specific side effect over a time period]/[sum of mice × time at risk during the same time period]) and cumulative incidence (CI = [number of mice with specific side effect at end time point]/[total number of mice at start]) were calculated for indicated side effects.

Pharmacokinetics of Anthracyclines in FVB Mice. Mice were housed in IVC under SPF conditions in the animal facility of the NKI (Amsterdam, The Netherlands). All mouse experiments were performed according to institutional and national guidelines and were approved by the Animal Ethics Committee of the NKI (Amsterdam, The Netherlands). Wild-type FVB mice were bred by the NKI mouse facility. Female mice (8 wk old) were i.v. injected with 5 mg/kg of Doxo, 5 mg/kg of Acla, or 5 mg/kg of diMe-doxo, with five mice per group. Four hours postinjection, animals were killed, and then heart, liver, kidney, spleen, reproductive organ, and plasma was collected. Hearts were cut into two pieces with coronal section. One piece was fixed in EAF for γH2AX staining. The other half of the heart and the rest of organs were weighed and frozen for the pharmacokinetics study. Doxo was measured by high performance liquid chromatography fluorescence detection as described before (67). Acla and diMe-Doxo were analyzed by LC-MS/MS. Sample pretreatment involved protein precipitation with acetonitrile: formic acid (99:1) containing 500 nM of Doxo as internal standard, followed by centrifugation (5 min, 20,000 × g) and dilution of the supernatant with water (1:3). Samples were centrifuged again, and an aliquot of 50 μL was injected into the LC-MS/MS system. Separation was done using an Extend C18 column (100 × 2.1 mm). Mobile phase A (0.1% formic acid in water) and B (methanol) was delivered at 0.4 mL/min at 20%B. Following injection, a linear gradient to 95%B in 2.5 min was applied, kept at 95% for 2 min, and then returned to 20%B. The API4000 MS (Sciex) was used in MRM mode; Acla: 812.5/333.1; diMe-Doxo: 571.9/99.9; and Doxo: 544.4/86.1).

PDX Mouse Model for AML. Mice were housed in IVC under SPF conditions in the animal facility of the VUmc (Amsterdam, The Netherlands). PDX mouse experiments were performed according to institutional and national guidelines and were approved by the Animal Ethics Committee of the VUmc (Amsterdam, The Netherlands). NOD/SCID/IL2r gamma null mice (Jackson Laboratory) (6 wk to 8 wk old) were i.v. injected with $0.7 × 10^6$ primary human AML cells per mouse 24 h post 200-cGy total irradiation. PB was taken via the tail vein and analyzed by flow cytometry for human AML cells, defined by > 0.7% of $hCD45^+$ cells. Six weeks after AML injection, mice were i.v. injected with 1.5 mg/kg of drug or saline weekly for the indicated times. Animals were monitored every other day. PB was taken from the tail vein and analyzed by flow cytometry at week 13. After killing, the hearts were collected for histopathological analysis, and BM was analyzed by flow cytometry.

MC38 Colon Carcinoma Mouse Model. Mice were housed in IVC under SPF conditions in the animal facility of Leiden University Medical Center (LUMC,

The Netherlands). Experiments were performed according to institutional and national guidelines and approved by the Animal Ethics Committee of LUMC (Leiden, The Netherlands). C57BL/6 female mice obtained from Charles River Laboratories, 8 wk to 10 wk old, were subcutaneously (s.c.) injected with 3×10^5 MC38 cells in the right flank of the mice. Tumor size was measured every 3 d to 4 d using a caliper. Mice were i.v. or retroorbitally injected with indicated doses of Doxo, Acla, diMe-doxo, or 5 mL/kg of saline every week for the indicated times. Mice were monitored twice per week. When the tumor exceeded 500 mm^3 or the body weight loss was more than 20%, the animal was killed by CO_2. Then the heart, reproductive organ, and tumor were collected, fixed in EAF fixative (ethanol/acetic acid/formaldehyde/saline at 40:5:10:45 vol/vol), and embedded in paraffin for histopathological analysis.

Echocardiography. Mice were housed in IVC under SPF conditions in the animal facility of LUMC (Leiden, The Netherlands). Experiment was performed according to institutional and national guidelines and approved by the Animal Ethics Committee of LUMC (Leiden, The Netherlands). Both male and female FVB N/ctr mice (8 wk old), were i.v. injected with 5 mg/kg of Doxo, 5 mg/kg of Acla, 5 mg/kg of diMe-doxo, or 5 mL/kg of saline every week for eight times. Animal welfare was monitored every other day. In vivo cardiac function was assessed by transthoracic echocardiograph. Mice were anesthetized with 2% isoflurane, depilated, and imaged in a supine position using a Vevo 3100 high-resolution ultrasound system, equipped with a 40-MHz center frequency linear array transducer (MX550D, FUJIFILM VisualSonics Inc.). Body temperature was kept at 37 °C, cardiac frequency was monitored with electrocardiogram and maintained between 400 bpm and 600 bpm. B-mode and M-mode echocardiographic images were obtained in short-axis (SAX) view at the midpapillary muscle level. Data were analyzed offline using VevoLAB software (FUIJIFILM VisualSonics), and left-ventricular function was assessed using EF and FS of at least three cardiac cycles on SAX M mode. To reconstruct the dimensions of the left ventricle and left atrium, 4D ultrasound imaging was performed by clamping the probe on a linearly translating step motor and positioning it parallel to the short axis of the left ventricle. System-integrated triggering between the motor and the probe resulted in automatically acquired high frame rate (300 frames per s) cardiac- and respiratory-gated cine loops with a 200-μm step size covering apex to base, that were spatiotemporally compiled into 4D data. The 3D images of the left ventricle and atrium were constructed by manual tracing offline using VevoLAB software (FUIJIFILM VisualSonics).

Western Blot and CFGE. Cells were treated with drugs at indicated doses for 2 h. Subsequently, drugs were removed by extensive washing, and cells were collected at indicated time points after drug removal and processed immediately for the assay. Cells were lysed directly in sodium dodecyl sulfate (SDS)-sample buffer (2% SDS, 10% glycerol, 5% β-mercaptoethanol, 60 mM Tris·HCl pH 6.8, and 0.01% bromophenol blue). Lysates were resolved by SDS/polyacrylamide gel electrophoresis followed by Western blotting. Primary antibodies used for blotting were γH2AX (1:1,000, 05-036, Millipore), β-actin (1:10000, A5441, Sigma), ubiquitin (1:500, P4D1, sc-8017, Santa Cruz), and alpha-tubulin (1:5,000, 11223-1-AP, Proteintech). DNA SDBs were quantified by CFGE, as described (46). Images were quantified with ImageJ.

Fractionation Assay. Endogenously tagged scarlet-H2B cells were treated for 1 h with 10 μM of the indicated drugs. Cells were washed and lysed directly in lysis buffer (50 mM Tris·HCl pH 8.0, 150 mM NaCl, 5 mM MgCl, 0.5% Nonidet P-40, 2.5% glycerol supplemented with protease inhibitors, 10 mM NMM and 10 μM MG132), collected, vortexed, and incubated for 10 min on ice. To collect the cytosolic fraction, samples were centrifuged for 10 min, 15,000 × g, 4 °C. Both nuclear (pellet) and cytosolic (supernatant) fractions were washed and prepared for Western blot analysis. Primary antibodies used for blotting were red fluorescent protein (RFP) (1:2,000, 6G6, Chromotek), lamin A/C (1:500, sc-20681, Santa Cruz), and Calnexin (1:1,000, C5C9, Cell signaling).

Comet Assay. Neutral comet assays were performed as described by Olive and Banáth (48). Pictures of individual cells were taken with a Zeiss AxioObserver Z1 inverted microscope equipped with a cooled Hamamatsu ORCA AG Black and White charge-coupled device camera and analyzed with CASP software 1.2.3b2 (casplab.com/).

Microscopy. Cells stably expressing PAGFP-H2A, PAGFP-H3, or PAGFP-H4 were used for histone eviction experiments. Photoactivation and time-lapse confocal imaging were performed as described (24). All live-cell imaging experiments were analyzed by a Leica SP8 confocal microscope system, 63× lens, equipped with a climate chamber. Loss of fluorescence from the

photoactivated region after different treatments was quantified using ImageJ software. For cytosolic H2B detection, endogenous tagged scarlet-H2B cells were seeded on coverslips. Upon treatment with 10 μM of the indicated drugs for 1 h, cells were fixed in paraformaldehyde (PFA) 4%, permeabilized with 0.1% Triton, and stained with anti-RFP (1:100, 6G6, Chomotek), goat-anti-mouse-Alexa Fluor 488 (1:400, Thermo Fisher Scientific), and Alexa Fluor 647 phalloidin (1:125, A22287, Thermo Fisher Scientific). Cells were analyzed by a Leica SP8 confocal microscope system, 63× lens. Cells were quantified using ImageJ software.

Cell Viability Assay. Indicated tumor cells or AML patient cells were seeded into 96-well plates. Twenty-four hours after seeding, cells were treated with indicated drugs for 2 h at concentrations corresponding to physiological levels of cancer patients at standard treatment (24). Subsequently, drugs were removed, and cells were left to grow for an additional 72 h. Cell viability was measured using the CellTiter-Blue viability assay (Promega). Relative survival was normalized to the untreated control and corrected for background signals.

Flow Cytometry for Measuring Drug Uptake in Cells. Cells were treated with 1 μM of drug for the indicated time points. Samples were washed, collected, and fixed with paraformaldehyde. Samples were analyzed by flow cytometry using BD FACS aria II, with 561-nm laser and 610/20-nm detector. Drug uptake was quantified using FlowJo software.

Detection of ROS. MelJuSo cells were treated with indicated drugs for 2 h followed by drug removal. Cells were collected immediately or 1 d after drug removal for analysis. Cells were then incubated with 10 μM 2′,7′-dichlorodihydrofluorescein diacetate (H_2DCFDA) (Invitrogen, D399) for 30 min at 37 °C in the dark, and fluorescence was analyzed with an LSRFortessa flow cytometer (BD Biosciences). Mean fluorescence intensity of H_2DCFDA was quantified using FlowJo software.

Flow Cytometry for Phenotyping AML Cells. Human AML cells were treated with indicated drug for 2 h, followed by extensive washing. Three days later, the cells were stained with anti-CD45-V500 (2D1, BD Bioscience, 1:20), anti-CD34-BV421 (581, BD Bioscience, 1:20), anti-CD38-APC (HB7, BD Bioscience, 1:50), anti-CD33-PE-Cy7 (p67.6, BD Bioscience, 1:20), anti-CD3-PE (SK7, BD Bioscience, 1:50), anti-CD19-APC-H7 (SJ25C1, BD Bioscience, 1:10), 7AAD (BD Bioscience, 1:10), and anti-CD11b-FITC (Bear1, BD Bioscience, 1:10) or anti-CD7-FITC (M-T701, BD Bioscience, 1:20) for 30 min. Then 15 μL of well-suspended flow count fluorospheres (Beckman Coulter) were added right before analysis by flow cytometry with BD Fortessa.

Assessing Drug Toxicity on hiPSC-Derived Cardiac Microtissues. The hiPSC-derived cardiac microtissues composed of hiPSC-derived cardiomyocytes and hiPSC-derived cardiac endothelial cells were generated as described (52, 53), with addition of stromal cells derived from hiPSC epicardial cells, differentiated in monolayer as described (54). For contraction analysis, microtissues were seeded on a Matrigel-coated 96-well plate (plastic, Black/Clear tissue culture treated plate) and imaged 24 h post drug treatment with 20 or 30 μM of the indicated drugs. The Horn-Schunck Vector Flow analysis method was used to detect changes in pixel displacements during contraction of the microtissues. The analysis package was developed with LabVIEW Motion and Vision (National Instruments). Images were collected at 100 frames per s with a Thor Labs camera DCC3260M (Thorlabs GmbH 85221) and a 10× objective phase contrast objective (Leica Inverted microscope IBDE). Microtissues were perfused with Tyrode's solution at 37 °C and paced at 1 Hz. Tyrode's solution contains 140 mM NaCl, 5.4 mM KCl, 1.8 mM CaCl$_2$, 1.0 mM MgCl$_2$, 5.5 mM glucose, and 5.0 mM Hepes; pH 7.4 (NaOH).

AML Patient Data Analysis. Patients with de novo geriatric AML treated between January 2014 and January 2019 in Ruijin hospitals were enrolled in this retrospectively study. This study was approved by the ethics committee of Ruijin Hospital, and all patients provided written informed consent. Patients in the Acla group were treated with CAG regimen (Ara-C 15–25 mg/m^2 injected s.c. every 12 h on days 1 to 14, Acla 20 mg/d infused i.v. on days 1 to 4, and granulocyte stimulating factor (G-CSF) 200 μg/m^2 administered s.c. daily on days 1 to 14). G-CSF was reduced, or temporarily stopped when neutrophilia was >5 × 10^9/L. Patients of Ida group were treated with IA regimen (Ida 6 mg/m^2/d to 10 mg/m^2/d infused i.v. on days 1 to 3 and Ara-C 100 mg/m^2/d to 200 mg/m^2/d on days 1 to 7). Cytogenetic risk was classified according to the modified Southwest Oncology Group criteria (68): 1) favorable risk, including

t (8, 21) and inv (16) or t (16, 16) (p13;q22); 2) unfavorable risk, including del(5q) or monosomy 5, monosomy 7 or del(7q), abnormal 3q, 9q, 11q, 21q, or 17p, t (6, 9), t (9, 22), and complex karyotypes (three or more unrelated chromosomes abnormal); and 3) intermediate risk, including normal karyotypes and all other anomalies. Mutations in the NPM1 and CEBPA, and for FLT3 internal tandem duplication, were tested. Integrated risk was classified according to ref. 69. CR was defined as <5% blast cells in normocellular BM, PB counts showing neutrophils $\geq 1 \times 10^9$/L, and platelet count $\geq 100 \times 10^9$/L, and the disappearance of all clinical signs of leukemia. Partial remission was defined as having <15% (and a 50% decrease in BM blasts) but >5% blasts or with <5% blasts but not reaching the CR criteria for blood cell count or clinical manifestation. For analysis of CR, missing data were imputed as no CR. The baseline characteristics and clinical outcomes of the patients are summarized in *SI Appendix*, Tables S2 and S3, respectively.

Quantification and Statistical Analysis. Each sample was assayed in biological triplicate, unless stated otherwise. All error bars denote SD. Statistical analyses were performed using Prism 7 and 8 software (Graphpad Inc.). Student's t test was used to compare two groups of independent samples. One-way ANOVA was used to compare more than two groups of independent samples. Two-way ANOVA with repeated measure analysis was used if the response of two drugs was compared over time. Kaplan–Meier

analysis and Log-rank (Mantel–Cox) test were used to evaluate the statistical significance for comparison of survival curves. Western blot and confocal data were quantified using ImageJ software. Significance is represented on the graphs as follows: ns, not significant; *$P < 0.05$; **$P < 0.01$; ***$P < 0.001$; ****$P < 0.0001$. No statistical methods were used to predetermine sample size.

Data Availability. All data support the findings of this study are included in the main text and *SI Appendix*. All procedures of experiments are described in detail in *Materials and Methods* and *SI Appendix*.

1. R. B. Weiss, The anthracyclines: Will we ever find a better doxorubicin? *Semin. Oncol.* **19**, 670–686 (1992).
2. D. Rayson *et al.*, Anthracycline-trastuzumab regimens for HER2/neu-overexpressing breast cancer: Current experience and future strategies. *Ann. Oncol.* **19**, 1530–1539 (2008).
3. M. Lotrionte *et al.*, Review and meta-analysis of incidence and clinical predictors of anthracycline cardiotoxicity. *Am. J. Cardiol.* **112**, 1980–1984 (2013).
4. K. Shan, A. M. Lincoff, J. B. Young, Anthracycline-induced cardiotoxicity. *Ann. Intern. Med.* **125**, 47–58 (1996).
5. K. Chatterjee, J. Zhang, N. Honbo, J. S. Karliner, Doxorubicin cardiomyopathy. *Cardiology* **115**, 155–162 (2010).
6. S. M. Swain, F. S. Whaley, M. S. Ewer, Congestive heart failure in patients treated with doxorubicin: A retrospective analysis of three trials. *Cancer* **97**, 2869–2879 (2003).
7. L. Liu *et al.*, Increasing aclarubicin dose in low-dose cytarabine and aclarubicin in combination with granulocyte colony-stimulating factor (CAG regimen) is efficacious as salvage chemotherapy for relapsed/refractory mixed-phenotype acute leukemia. *Leuk. Res.* **39**, 805–811 (2015).
8. Q. Qu, L. Liu, Y. Zhang, X. Li, D. Wu, Increasing aclarubicin dosage of the conventional CAG (low-dose cytarabine and aclarubicin in combination with granulocyte colony-stimulating factor) regimen is more efficacious as a salvage therapy than CAG for relapsed/refractory acute myeloid leukemia. *Leuk. Res.* **39**, 1353–1359 (2015).
9. E. Sadurska, Current views on anthracycline cardiotoxicity in childhood cancer survivors. *Pediatr. Cardiol.* **36**, 1112–1119 (2015).
10. D. A. Mulrooney *et al.*, Cardiac outcomes in a cohort of adult survivors of childhood and adolescent cancer: Retrospective analysis of the Childhood Cancer Survivor Study cohort. *BMJ* **339**, b4606 (2009).
11. M. A. Grenier, S. E. Lipshultz, Epidemiology of anthracycline cardiotoxicity in children and adults. *Semin. Oncol.* **25** (suppl. 10), 72–85 (1998).
12. M. Volkova, R. Russell 3rd, Anthracycline cardiotoxicity: Prevalence, pathogenesis and treatment. *Curr. Cardiol. Rev.* **7**, 214–220 (2011).
13. D. K. Shakir, K. I. Rasul, Chemotherapy induced cardiomyopathy: Pathogenesis, monitoring and management. *J. Clin. Med. Res.* **1**, 8–12 (2009).
14. A. R. Mistry *et al.*, DNA topoisomerase II in therapy-related acute promyelocytic leukemia. *N. Engl. J. Med.* **352**, 1529–1538 (2005).
15. M. J. Ratain, J. D. Rowley, Therapy-related acute myeloid leukemia secondary to inhibitors of topoisomerase II: From the bedside to the target genes. *Ann. Oncol.* **3**, 107–111 (1992).
16. R. E. Smith, J. Bryant, A. DeCillis, S. Anderson; National Surgical Adjuvant Breast and Bowel Project Experience, Acute myeloid leukemia and myelodysplastic syndrome after doxorubicin-cyclophosphamide adjuvant therapy for operable breast cancer: The National Surgical Adjuvant Breast and Bowel Project Experience. *J. Clin. Oncol.* **21**, 1195–1204 (2003).
17. M. André *et al.*; Groupe D'Etude Des Lymphomes De L'Adulte, Second cancers and late toxicities after treatment of aggressive non-Hodgkin lymphoma with the ACVBP regimen: A GELA cohort study on 2837 patients. *Blood* **103**, 1222–1228 (2004).
18. S. Kayser *et al.*; German-Austrian AMLSG, The impact of therapy-related acute myeloid leukemia (AML) on outcome in 2853 adult patients with newly diagnosed AML. *Blood* **117**, 2137–2145 (2011).
19. E. Hulegårdh *et al.*, Characterization and prognostic features of secondary acute myeloid leukemia in a population-based setting: A report from the Swedish Acute Leukemia Registry. *Am. J. Hematol.* **90**, 208–214 (2015).
20. C. A. Felix, Secondary leukemias induced by topoisomerase-targeted drugs. *Biochim. Biophys. Acta* **1400**, 233–255 (1998).
21. R. Govindan, D. Morgensztern, *Devita, Hellman, and Rosenberg's Cancer: Principles and Practice of Oncology Review*, (Wolters Kluwer Health, 2012).
22. K. M. Tewey, T. C. Rowe, L. Yang, B. D. Halligan, L. F. Liu, Adriamycin-induced DNA damage mediated by mammalian DNA topoisomerase II. *Science* **226**, 466–468 (1984).
23. G. L. Chen *et al.*, Nonintercalative antitumor drugs interfere with the breakage-reunion reaction of mammalian DNA topoisomerase II. *J. Biol. Chem.* **259**, 13560–13566 (1984).
24. B. Pang *et al.*, Drug-induced histone eviction from open chromatin contributes to the chemotherapeutic effects of doxorubicin. *Nat. Commun.* **4**, 1908 (2013).
25. D. J. Girling; Medical Research Council Lung Cancer Working Party, Comparison of oral etoposide and standard intravenous multidrug chemotherapy for small-cell lung cancer: A stopped multicentre randomised trial. *Lancet* **348**, 563–566 (1996).
26. W. K. Hong *et al.*, Etoposide combined with cyclophosphamide plus vincristine compared with doxorubicin plus cyclophosphamide plus vincristine and with high-dose cyclophosphamide plus vincristine in the treatment of small-cell carcinoma of the lung: A randomized trial of the Bristol Lung Cancer Study Group. *J. Clin. Oncol.* **7**, 450–456 (1989).
27. F. Yang, C. J. Kemp, S. Henikoff, Doxorubicin enhances nucleosome turnover around promoters. *Curr. Biol.* **23**, 782–787 (2013).
28. E. Nesher *et al.*, Role of chromatin damage and chromatin trapping of FACT in mediating the anticancer cytotoxicity of DNA-binding small-molecule drugs. *Cancer Res.* **78**, 1431–1443 (2018).
29. B. Pang, J. de Jong, X. Qiao, L. F. Wessels, J. Neefjes, Chemical profiling of the genome with anti-cancer drugs defines target specificities. *Nat. Chem. Biol.* **11**, 472–480 (2015).
30. G. Wei *et al.*, A meta-analysis of CAG (cytarabine, aclarubicin, G-CSF) regimen for the treatment of 1029 patients with acute myeloid leukemia and myelodysplastic syndrome. *J. Hematol. Oncol.* **4**, 46 (2011).
31. J. Jin *et al.*, Homoharringtonine-based induction regimens for patients with de-novo acute myeloid leukaemia: A multicentre, open-label, randomised, controlled phase 3 trial. *Lancet Oncol.* **14**, 599–608 (2013).
32. J. Jonkers *et al.*, Synergistic tumor suppressor activity of BRCA2 and p53 in a conditional mouse model for breast cancer. *Nat. Genet.* **29**, 418–425 (2001).
33. D. Ben-Yehuda *et al.*, Microsatellite instability and p53 mutations in therapy-related leukemia suggest mutator phenotype. *Blood* **88**, 4296–4303 (1996).
34. T. N. Wong *et al.*, Role of TP53 mutations in the origin and evolution of therapy-related acute myeloid leukaemia. *Nature* **518**, 552–555 (2015).
35. A. Gabizon, A. Meshorer, Y. Barenholz, Comparative long-term study of the toxicities of free and liposome-associated doxorubicin in mice after intravenous administration. *J. Natl. Cancer Inst.* **77**, 459–469 (1986).
36. D. Hanahan, R. A. Weinberg, Hallmarks of cancer: The next generation. *Cell* **144**, 646–674 (2011).
37. J. C. Teepen *et al.*; DCOG LATER Study Group, Long-term risk of subsequent malignant neoplasms after treatment of childhood cancer in the DCOG LATER study cohort: Role of chemotherapy. *J. Clin. Oncol.* **35**, 2288–2298 (2017).
38. T. O. Henderson *et al.*, Breast cancer risk in childhood cancer survivors without a history of chest radiotherapy: A report from the Childhood Cancer Survivor Study. *J. Clin. Oncol.* **34**, 910–918 (2016).
39. O. Hequet *et al.*, Subclinical late cardiomyopathy after doxorubicin therapy for lymphoma in adults. *J. Clin. Oncol.* **22**, 1864–1871 (2004).
40. S. Fujihira *et al.*, The high incidence of atrial thrombosis in mice given doxorubicin. *Toxicol. Pathol.* **21**, 362–368 (1993).
41. E. A. Lefrak, J. Pitha, S. Rosenheim, J. A. Gottlieb, A clinicopathologic analysis of adriamycin cardiotoxicity. *Cancer* **32**, 302–314 (1973).
42. S. Zhao *et al.*, Periostin expression is upregulated and associated with myocardial fibrosis in human failing hearts. *J. Cardiol.* **63**, 373–378 (2014).
43. O. Lenčová-Popelová *et al.*, Molecular remodeling of left and right ventricular myocardium in chronic anthracycline cardiotoxicity and post-treatment follow up. *PLoS One* **9**, e96055 (2014).
44. D. Ogawara, M. Fukuda, Y. Nakamura, S. Kohno, Efficacy and safety of amrubicin hydrochloride for treatment of relapsed small cell lung cancer. *Cancer Manag. Res.* **2**, 191–195 (2010).

45. P. A. Speth, Q. G. van Hoesel, C. Haanen, Clinical pharmacokinetics of doxorubicin. *Clin. Pharmacokinet.* **15**, 15–31 (1988).

46. D. Wlodek, J. Banáth, P. L. Olive, Comparison between pulsed-field and constant-field gel electrophoresis for measurement of DNA double-strand breaks in irradiated Chinese hamster ovary cells. *Int. J. Radiat. Biol.* **60**, 779–790 (1991).

47. S. Neijenhuis et al., Mechanism of cell killing after ionizing radiation by a dominant negative DNA polymerase beta. *DNA Repair (Amst.)* **8**, 336–346 (2009).

48. P. L. Olive, J. P. Banáth, The comet assay: A method to measure DNA damage in individual cells. *Nat. Protoc.* **1**, 23–29 (2006).

49. L. J. Kuo, L. X. Yang, Gamma-H2AX—A novel biomarker for DNA double-strand breaks. *In Vivo* **22**, 305–309 (2008).

50. T. Suzuki, S. Minamide, T. Iwasaki, H. Yamamoto, H. Kanda, Cardiotoxicity of a new anthracycline derivative (SM-5887) following intravenous administration to rabbits: Comparative study with doxorubicin. *Invest. New Drugs* **15**, 219–225 (1997).

51. P. V. Sanchez et al., A robust xenotransplantation model for acute myeloid leukemia. *Leukemia* **23**, 2109–2117 (2009).

52. E. Giacomelli, M. Bellin, V. V. Orlova, C. L. Mummery, Co-differentiation of human pluripotent stem cells-derived cardiomyocytes and endothelial cells from cardiac mesoderm provides a three-dimensional model of cardiac microtissue. *Curr. Protoc. Hum. Genet.* **95**, 21.9.1-21.9.22 (2017).

53. E. Giacomelli et al., Three-dimensional cardiac microtissues composed of cardiomyocytes and endothelial cells co-differentiated from human pluripotent stem cells. *Development* **144**, 1008–1017 (2017).

54. J. A. Guadix et al., Human pluripotent stem cell differentiation into functional epicardial progenitor cells. *Stem Cell Reports* **9**, 1754–1764 (2017).

55. L. Sala et al., MUSCLEMOTION: A versatile open software tool to quantify cardiomyocyte and cardiac muscle contraction in vitro and in vivo. *Circ. Res.* **122**, e5–e16 (2018).

56. M. Aapro et al., Anthracycline cardiotoxicity in the elderly cancer patient: A SIOG expert position paper. *Ann. Oncol.* **22**, 257–267 (2011).

57. C. E. Myers et al., Adriamycin: The role of lipid peroxidation in cardiac toxicity and tumor response. *Science* **197**, 165–167 (1977).

58. S. M. Swain et al., Cardioprotection with dexrazoxane for doxorubicin-containing therapy in advanced breast cancer. *J. Clin. Oncol.* **15**, 1318–1332 (1997).

59. E. Martin et al., Evaluation of the topoisomerase II-inactive bisdioxopiperazine ICRF-161 as a protectant against doxorubicin-induced cardiomyopathy. *Toxicology* **255**, 72–79 (2009).

60. C. Myers et al., A randomized controlled trial assessing the prevention of doxorubicin cardiomyopathy by N-acetylcysteine. *Semin. Oncol.* **10** (suppl. 1), 53–55 (1983).

61. K. Hashimoto, K. Ito, Y. Ishimori, Novel DNA sensor for electrochemical gene detection. *Anal. Chim. Acta* **286**, 219–224 (1994).

62. A. A. Gabizon, Y. Patil, N. M. La-Beck, New insights and evolving role of pegylated liposomal doxorubicin in cancer therapy. *Drug Resist. Updat.* **29**, 90–106 (2016).

63. J. van Asperen, O. van Tellingen, F. Tijssen, A. H. Schinkel, J. H. Beijnen, Increased accumulation of doxorubicin and doxorubicinol in cardiac tissue of mice lacking mdr1a P-glycoprotein. *Br. J. Cancer* **79**, 108–113 (1999).

64. U. H. Steinhorst, E. P. Chen, S. F. Freedman, R. Machemer, D. L. Hatchell, Growth inhibition of human Tenon's capsule fibroblasts and rabbit dermal fibroblasts with non-carcinogenic N-alkylated anthracyclines. *Graefes Arch. Clin. Exp. Ophthalmol.* **232**, 347–354 (1994).

65. A. Schaefer et al., Decreased resistance to N,N-dimethylated anthracyclines in multidrug-resistant Friend erythroleukemia cells. *Cancer Chemother. Pharmacol.* **31**, 301–307 (1993).

66. M. Binaschi, G. Capranico, L. Dal Bo, F. Zunino, Relationship between lethal effects and topoisomerase II-mediated double-stranded DNA breaks produced by anthracyclines with different sequence specificity. *Mol. Pharmacol.* **51**, 1053–1059 (1997).

67. J. van Asperen, O. van Tellingen, J. H. Beijnen, Determination of doxorubicin and metabolites in murine specimens by high-performance liquid chromatography. *J. Chromatogr. B Biomed. Sci. Appl.* **712**, 129–143 (1998).

68. M. L. Slovak et al., Karyotypic analysis predicts outcome of preremission and postremission therapy in adult acute myeloid leukemia: A Southwest Oncology Group/Eastern Cooperative Oncology Group study. *Blood* **96**, 4075–4083 (2000).

69. H. Döhner et al.; European LeukemiaNet, Diagnosis and management of acute myeloid leukemia in adults: Recommendations from an international expert panel, on behalf of the European LeukemiaNet. *Blood* **115**, 453–474 (2010).